Magnetic field production via the Weibel instability in interpenetrating plasma flows

C. M. Huntington, M. J.-E. Manuel, J. S. Ross, S. C. Wilks, F. Fiuza, H. G. Rinderknecht, H.-S. Park, G. Gregori, D. P. Higginson, J. Park, B. B. Pollock, B. A. Remington, D. D. Ryutov, C. Ruyer, Y. Sakawa, H. Sio, A. Spitkovsky, G. F. Swadling, H. Takabe, and A. B. Zylstra

Citation: Physics of Plasmas **24**, 041410 (2017); doi: 10.1063/1.4982044
View online: http://dx.doi.org/10.1063/1.4982044
View Table of Contents: http://aip.scitation.org/toc/php/24/4
Published by the American Institute of Physics

Magnetic field production via the Weibel instability in interpenetrating plasma flows

C. M. Huntington,[1] M. J.-E. Manuel,[2] J. S. Ross,[1] S. C. Wilks,[1] F. Fiuza,[3] H. G. Rinderknecht,[1] H.-S. Park,[1] G. Gregori,[4] D. P. Higginson,[1] J. Park,[5] B. B. Pollock,[1] B. A. Remington,[1] D. D. Ryutov,[1] C. Ruyer,[3] Y. Sakawa,[6] H. Sio,[7] A. Spitkovsky,[5] G. F. Swadling,[1] H. Takabe,[6] and A. B. Zylstra[8]

[1]*Lawrence Livermore National Laboratory, Livermore, California 94551, USA*
[2]*University of Michigan, Ann Arbor, Michigan 48109, USA*
[3]*Stanford Linear Accelerator Laboratory, Menlo Park, California 94025, USA*
[4]*University of Oxford, Parks Road, Oxford OX1 3PU, United Kingdom*
[5]*Princeton University, Princeton, New Jersey 08544, USA*
[6]*Osaka University, Osaka, Japan*
[7]*Massachusetts Institute of Technology, Cambridge, Massachusetts 02139, USA*
[8]*Los Alamos National Laboratory, Los Alamos, New Mexico 87507, USA*

(Received 16 January 2017; accepted 4 April 2017; published online 26 April 2017)

Many astrophysical systems are effectively "collisionless," that is, the mean free path for collisions between particles is much longer than the size of the system. The absence of particle collisions does not preclude shock formation, however, as shocks can be the result of plasma instabilities that generate and amplify electromagnetic fields. The magnetic fields required for shock formation may either be initially present, for example, in supernova remnants or young galaxies, or they may be self-generated in systems such as gamma-ray bursts (GRBs). In the case of GRB outflows, the Weibel instability is a candidate mechanism for the generation of sufficiently strong magnetic fields to produce shocks. In experiments on the OMEGA Laser, we have demonstrated a quasi-collisionless system that is optimized for the study of the non-linear phase of Weibel instability growth. Using a proton probe to directly image electromagnetic fields, we measure Weibel-generated magnetic fields that grow in opposing, initially unmagnetized plasma flows. The collisionality of the system is determined from coherent Thomson scattering measurements, and the data are compared to similar measurements of a fully collisionless system. The strong, persistent Weibel growth observed here serves as a diagnostic for exploring large-scale magnetic field amplification and the microphysics present in the collisional–collisionless transition. *Published by AIP Publishing.* [http://dx.doi.org/10.1063/1.4982044]

I. INTRODUCTION

Collisionless shocks occur in systems where the low ambient particle density may preclude frequent particle-particle collisions, but is nevertheless sufficient for electromagnetic instabilities to grow. Collisionless shocks are viewed as a dominant source of energetic cosmic rays, and there is now observational evidence of cosmic ray acceleration in supernova remnant shocks.[1] However, important aspects of the particle acceleration mechanism are not fully understood.[2–8] Outstanding questions include the detailed processes responsible for shock formation and for the generation of strong waves and magnetic turbulence capable of scattering particles in the vicinity of shock.

One proposed mechanism for converting the kinetic energy of a streaming plasma flow into magnetic energy capable of sustaining a collisionless shock is the electromagnetic Weibel instability.[9] Weibel-generated magnetic fields grow from anisotropies in the velocity distribution of the flow, and despite the small-scale structure of the magnetic fields (initially growing at the length scale of the plasma skin depth c/ω_{pi}), the amplification of the fields in time can produce effectively "collisionless" shocks. In the case of supernovae explosions, the plasma outflow interacting with the lower density material surrounding the collapsed star may generate collisionless shocks.[10,11] In some cases, strong pre-existing magnetic fields are present in these systems. If so, these background fields may serve to moderate filamentation instabilities or generate competing instabilities that supersede filamentation as the fastest growing mode.[12,13] Laboratory experiments to study collisionless shocks with pre-imposed initial magnetic fields are an area of active development.[14–16]

Weibel instabilities will also grow in the relativistic flows from gamma-ray bursts (GRBs),[5,17,18] where the self-generated fields may be the dominant source of magnetic energy in the system.[19–21] Charged particle oscillations in the resulting tightly "tangled" magnetic fields that wrap around current filaments have even been proposed as the origin of the radiation signature observed in the late stages of GRB emission.[22–24] These relativistic flows have been explored in detail via numerical simulations, which have confirmed the role of the Weibel instability in producing magnetic energy densities on the order of 1%–10% of the kinetic energy density in the system,[25] in slowing down the flows to form a shock,[3,26,27] and in providing effective scattering for particle acceleration processes.[5,6,18,25,28] Relativistic particle flows in laboratory experiments to date fall short of the system size required for shock formation.[29–31] However, astrophysically relevant non-relativistic plasma flow can be achieved in the laboratory and

provide a valuable testbed for the physics of magnetic field generation from filamentation instabilities.

Using the Omega Laser Facility, we have performed experiments that achieve collisionless conditions by driving fast, low-density plasma flows.[32–34] In the laboratory, the required condition for a system to be collisionless is that the Coulomb mean-free-path for collisions (λ_{mfp}) must be much longer than the spatial scale of the interacting plasmas, l_{int} (in the laboratory this is the experimental scale).[32] The mean free path is a strong function of the plasma flow velocity v, but also depends on the ion density n_i, and goes as

$$\lambda_{mfp} \propto \left(\frac{A}{Z^2}\right)^2 \frac{v^4}{n_i}, \tag{1}$$

where A and Z are the atomic weight and charge of the ion species in the flow. An experiment designed to minimize collisional effects must drive a fast, low-density plasma flow, and in previous experiments performed on OMEGA, the mean free path exceeded the system size by greater than a factor of 10 (see Refs. 32–35 and Table I for relevant metrics from those experiments).

These fast, collisionless plasma flows are susceptible to several instabilities, including the Weibel instability. The growth rate of the Weibel instability is proportional to the flow velocity and the inverse ion skin depth, that is:

$$\gamma_W \propto v\frac{\omega_{pi}}{c} = \frac{v}{c}\sqrt{\frac{4\pi n_i Z^2 q_e^2}{A m_p}}. \tag{2}$$

Here, ω_{pi} is the plasma frequency, and m_p and q_e are the proton mass and electron charge, respectively (other terms are as above). The small-scale, tangled magnetic fields generated by the Weibel (and other filamentation instabilities) can be visualized with charged particle imaging, employing quasi-monoenergetic protons produced in D^3He nuclear reactions (see Ref. 36 for details of this technique). The resulting images reveal a complex, Weibel-generated magnetic structure in the OMEGA experiments, and comparison of these images to 3D simulations indicates a strong component of self-generated magnetic energy, approaching 1% of the total kinetic energy of the system. Similar work on OMEGA EP[37,38] has demonstrated the range of conditions where these electromagnetic (EM) instabilities can give rise to large scale structures in initially homogenous flow.

We can see from Eqs. (1) and (2) that optimizing an experiment to promote strong Weibel growth includes increasing the ion density n_i, which in turn serves to decrease the mean free path for collisions λ_{mfp}. In the work presented here, we have increased the ion density such that the system is only marginally collisionless ($\lambda_{mfp} \sim 5$ mm, on the order of the experimental system size $l_{int} = 5$ mm), but in doing so, strongly promote Weibel instability growth. We note that collisional effects from ion-ion and electron-ion collisions can, in some cases, stabilize filamentation instabilities, but this occurs at lower temperatures than the work presented here.[39] Temperature and density in the experiments were measured with collective Thomson scattering (TS), and proton radiographs from the system were compared to previous measurements of Weibel growth in a lower density (more collisionless) system, revealing an increased duration of Weibel instability growth before the conclusion of the experiment.

II. EXPERIMENTAL CONFIGURATION

The plasma flows in this experiment were generated by laser irradiation of a flat plastic (CH) target with several beams from the OMEGA Laser. Each beam delivered 500 J to a spot approximately 300 μm in diameter, and was shaped and smoothed by a distributed phase plate (DPP). Each pulse was 1 ns, and each beam therefore generated an intensity of $\sim 7 \times 10^{14}$ W/cm^2 on target. With 5–7 beams participating, the mid-10^{15} W/cm^2 intensity quickly heats the electrons, which are ablated from the surface and quickly begin to cool adiabatically. The ions follow the electrons with velocity exceeding 1000 km/s, and when viewed from a location several mm from the laser spot, the expanding plasma is approximately spherical.

To create opposing flows, the system just described is mirrored around a central "interaction point," so that the flow from each target streams into this point from each side. In previous experiments performed in this configuration,[32–35] the separation of the plasma sources was 8 mm (each was 4 mm from the interaction point; hereafter called "8 mm system"). In recent experiments described here, the separation between the targets was reduced to 5 mm (each was 2.5 mm from the interaction region; "5 mm system"), with the intention of increasing the ion density at the central point. In order to accommodate this geometry, the number of beams available to drive each target was reduced to 5, yielding 2.5 kJ of energy on each target.

Two primary diagnostics are employed on each shot. Measurements of the plasma conditions in both single and opposing-flow systems (at a separation of 8 mm) have been studied extensively using the coherent Thomson scattering (TS) diagnostic, and the method and measurements have been described in detail in Ref. 32. In that work, the TS k vector (where $k = k_s - k_o$; k_o is the wave number of the probe

TABLE I. Relevant plasma conditions for present and upcoming collisionless shock experiments. The electron density n_e is the two-stream density, the carbon ion density is $n_i = n_e/14$, and both have units of 10^{18} cm^{-3}. Note that the NIF values are taken from 2D hydrodynamic simulations, as the NIF Thomson scattering diagnostic is under construction.

Facility	Target sep. (mm)	Energy (kJ)	n_e	n_i	Velocity (km/s)	Temp (eV)	$\lambda_{mfp:CC}$ (mm)	c/ω_{pi} (μm)	γ_W (ns^{-1})
Omega[34,35]	8	4	10	0.7	800	1000	80	130	8
Omega	8	3.5	12	0.9	680	670	35	120	8
Omega	5	2.5	44	3	570	450	5	60	12
NIF (sim.)	10	250	150	11	1000	…	4	20	40

beam and k_s is the wave number of the scattered light) was aligned parallel to the plasma flow. In order to field the opposing plasma flows at 5 mm separation, the experiment was rotated about the interaction point such that the TS k vector was at perpendicular to the flow direction. The scattering vectors for the 5 and 8 mm systems are shown relative to the flow directions in Fig. 1.

To measure the electromagnetic structures that are formed in the interpenetrating plasma flows, we employ an imploding D^3He capsule and a charged particle track detector along an axis through the interaction point and perpendicular to the plasma flow direction. Fourteen Omega beams were used to compress the capsule, which was approximately 400 μm diameter glass capsule filled with 12 atm of deuterium gas and 6 atm of ^{3}He. Upon implosion, the capsule produces quasi-monoenergetic proton populations at 3 MeV and 14.7 MeV,[40] which emanate from a source ~45 μm FWHM. The protons are deflected by the EM fields in the plasma flows and are collected by a nuclear track detector (CR39) positioned 290 mm from the plasma interaction point, imaging the system with a magnification of 30. The resulting image shows regions of higher and lower proton flux, as a result of the deflections by EM fields. By comparing these images with synthetic proton images from 3D particle-in-cell (PIC) codes, the 2D map of the 3D field structure can be related to EM field strength and total magnetic energy in the system.[34,41,42]

III. DATA AND MODELING

In the 8 mm system, eight Omega beams were incident on each target, for a total energy of 4 kJ. Under these conditions, the maximum incoming electron density from each flow was measured by Thomson scattering to be $\sim 5 \pm 1 \times 10^{18}\,\mathrm{cm}^{-3}$ and was observed to reach the interaction point at approximately 5 ns, suggesting a velocity of 800 km/s for these particles in the densest portion of the flow. When the laser irradiated surfaces were positioned at 2.5 mm from the interaction point and the total energy on each surface decreased to 2.5 kJ, a four-fold increase in density was measured, approximately $20 \pm 2.5 \times 10^{18}\,\mathrm{cm}^{-3}$. The peak density in this case was recorded at 4 ns, indicating that the velocity of the particles at the peak density was ~650 km/s (see Fig. 2). This is somewhat slower than the velocity recorded at 8 mm separation, attributed to the decreased laser energy at the smaller separation. Thus, despite the reduced energy, moving the origin points of the interpenetrating plasmas closer together leads to a significant increase in the density.

To understand the longer-time evolution of the system, outside of the time range where TS data were collected, a series of simulations were performed. The radiation hydrodynamics simulation code HYDRA[43] was used to simulate the plasma plume that develops from the laser hitting a single deuterated plastic (CD) foil in cylindrical geometry run with a fixed grid of 180×600 in size. Separate electron and ion temperatures were used, and CD was used as a surrogate for CH in the simulations. Vacuum was modeled as a low density hydrogen gas. The two groups of laser beams, incident at 40° and 50°, were represented as 10,000 rays that were traced through the plasma, and deposited energy via inverse bremsstrahlung and a simplified model of resonance absorption. The laser parameters were identical to those used in the experiment, except that only 60% of the laser energy was used, to account for backscatter and other energy coupling losses that occur in the experiments, but are not otherwise included in HYDRA. Tabular equations of state, opacities, and thermal conductivities were used. Radiation transport was modeled using diffusive multi-group radiation

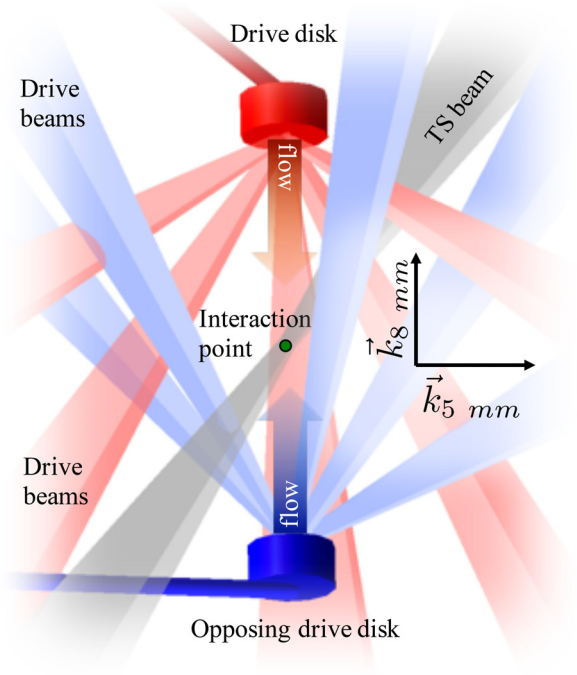

FIG. 1. The experimental geometry is shown, with 5 drive beams on each target. Opposing flows are generated at equal distances from a central interaction point, where the Thomson scattering probe beam and the proton imaging diagnostics are pointed. Because the TS diagnostic collection optics are in a fixed location, a different scattering vector **k** was used for the 5 mm and 8 mm separations, as indicated by $\mathbf{k}_{5\,\mathrm{mm}}$ and $\mathbf{k}_{8\,\mathrm{mm}}$.

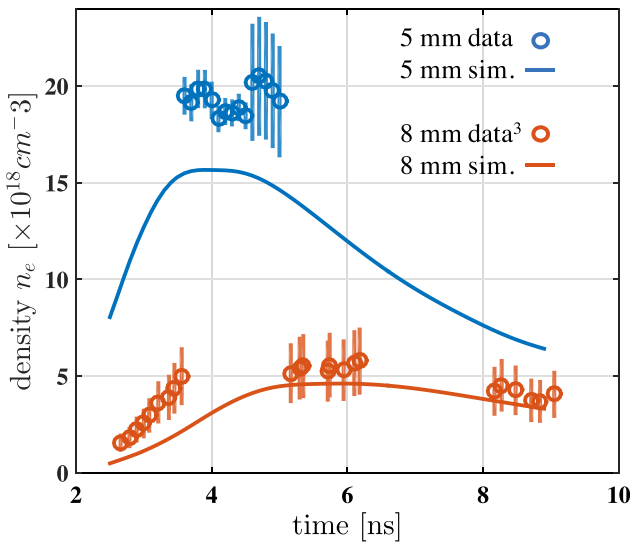

FIG. 2. The electron density measured using TS diagnostic is shown. In each case, the measurement is taken at the interaction region, midway between the opposing plasma sources (i.e., 2.5 mm for the 5 mm separation and 4 mm for the 8 mm separation). Also shown are the results of the 2D radiation hydrodynamics simulation at 2.5 mm from the target surface. The 8 mm data have been adapted from Ref. 32.

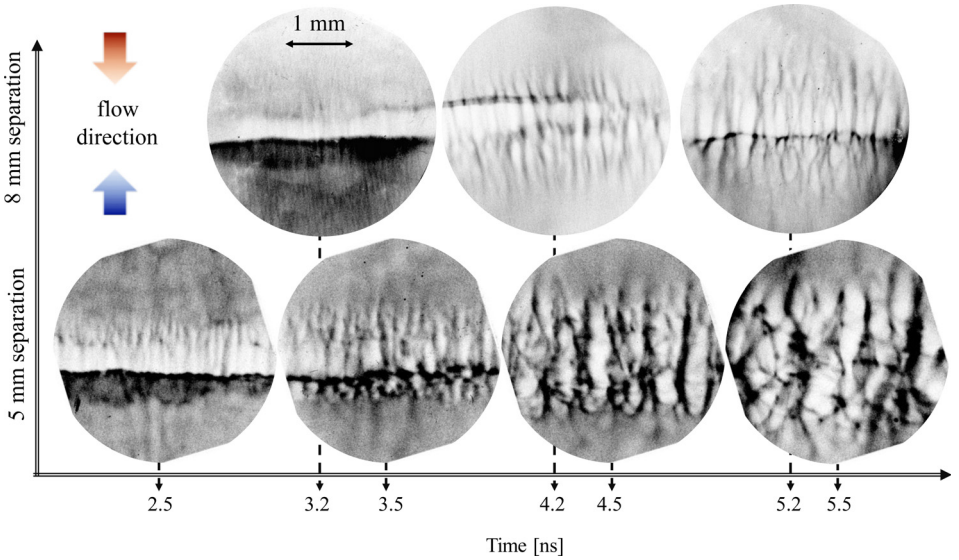

FIG. 3. Proton radiographs taken a four times, measured from the beginning the irradiation of the target surfaces. In each image, the opposing flows are generated at the top and bottom of the frame. At 2.5 ns, the fastest particles have reached the interaction region and the smallest observed filaments are generated. Over the next 3 ns, the spatial scale of the filaments perpendicular to the flow direction grows, as filaments merge up to longer wavelengths. Additionally, the extent of the strongly magnetized region grows along the plasma flow direction, as particles with slower initial velocity interact with the opposing flow. Note, the field of view of each image is approximately 3.3 mm.

with 16 groups that used tabular opacities. These simulations provide useful initial conditions for 3D particle-in-cell (PIC) calculations of the electromagnetic structure, as revealed by proton imaging and described below.

In addition to Thomson scattering measurements, proton radiographs were collected on each shot and spanned a range of times after the start of the drive pulses. In the 5 mm system, proton images were taken at 1 ns increments over from 2.5–5.5 ns, as shown in the bottom row of images in Fig. 3. The top row in Fig. 3 shows images taken from the 8 mm system, and were collected on previous OMEGA shot days, as described in Refs. 33 and 34. At the earliest time (2.5 ns after the drive), the opposing plasma flows have not reached peak density, but the flow is fast, with velocities of at least 1000 km/s. As shown in Eq. (2), the fast flow helps drive Weibel-generated filaments along the flow axis in a region with an axial extent of approximately 1 mm. When imaged 1 ns later, the filamentary region has grown along the axial direction, and the average spacing between the filaments increased from 125 μm to 170 μm (the measurement technique employed here is described in Ref. 33). Images taken at subsequent times showed this continuing trend towards larger filaments that extending a longer distance along the plasma flow vector.

As shown in Fig. 4, the filamentation wavelength grows approximately linearly in time during the non-linear stage of the instability (i.e., after saturation) in the 5 mm system, and unlike the measurements of wavelength growth in the 8 mm system, the filament scale length does not plateau over the time range of the measurements. At the larger 8 mm separation, it is likely that the expanding plasma has dropped in density such that there is insufficient inflow of material at the interaction point to sustain the instability. However, nearly linear growth of the filament wavelength is observed over the entire observed duration in the 5 mm system, with a rate similar to the *initial* rate at 8 mm, as indicated by the dashed lines in Fig. 4.

To compare the evolution of the Weibel instability and generation of magnetic fields with our experimental data. We have performed detailed 2D particle-in-cell (PIC) simulations of the interaction of non-relativisitic counter-streaming plasma flows. The simulations were performed with the fully relativistic, electromagnetic, and massively parallel PIC code OSIRIS.[44,45] Given the need to resolve both electrons and ion dynamics in full-PIC simulations and the large system size involved in such simulations, common strategies were adopted to reduce the computational load and still allow for the scaling of the numerical results to the experiments. A single ion species (carbon) is used with a reduced mass to charge ratio of $m_i/(m_e Z) = 512$. Additionally, a flow velocity of $0.1c$ is used, which preserves the non-relativistic nature of the interaction but greatly speeds up the simulation when compared to a flow velocity of $0.003c$. This strategy is reasonably justified in regimes dominated by the Weibel (electromagnetic) instability, as the case of our experiments. For such conditions, it can be shown analytically that the behavior of the system can be scaled for different velocities.[46] The large mass ratio used guarantees clear separation of scales between electrons and ions. The simulation results are then

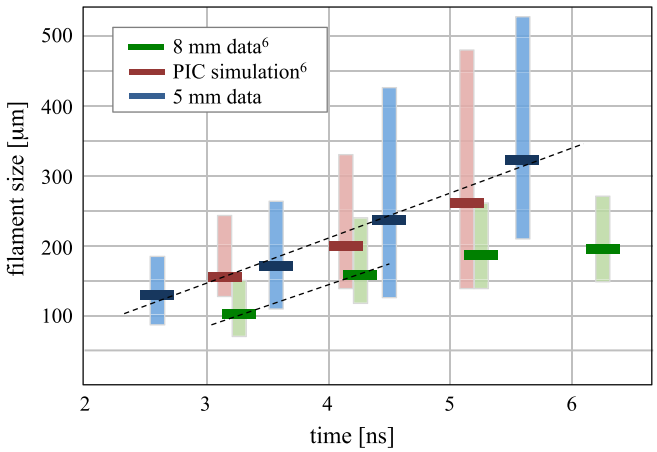

FIG. 4. The scale of the filamentary structure observed in the time sequence of proton radiographs is compared for the system at 5 mm separation and 8 mm separation. Here, the horizontal bars represent the average measured filament separation, with vertical bars indicating maximum and minimum values observed. Also shown in the same analysis of synthetic radiographs generated from 3D PIC calculations, as described in Ref. 34. When the plasma sources are closer, the increased density and decreased r^{-3} divergence of the ion flow yield larger Weibel growth features.

scaled based on the ion dynamics to the experimental conditions, for a single flow electron density of $n_e = 10^{19}\,\mathrm{cm}^{-3}$ and velocity $v = 1000\,\mathrm{km/s}$. The simulation box size is $90 \times 45(c/\omega_{pi})^2 \simeq 9.0 \times 4.5\,\mathrm{mm}^2$, uses 8192×4096 cells, and 64 particle per cell per species. In the simulation, the direction of the flows is horizontal (along x), and the initial flow density and velocity are constant within each flow.

Figure 5 illustrates the simulation results scaled to our experimental conditions. At early times (Fig. 5(a) at $t = 3.3\,\mathrm{ns}$), we observe the development of ordered magnetic field filaments with wave-vector transverse to the flow direction and with wavelength of $\sim c/\omega_{pi} \sim 0.1\,\mathrm{mm}$. The magnetic field at saturation reaches 0.2 MG. At later times, the magnetic filament evolution becomes nonlinear. We first observe filament merging and growth of the magnetic wavelength to $\sim 150\ \mu\mathrm{m}$ by 4.3 ns. At even later times ($t = 5.3\,\mathrm{ns}$), we observe further growth of the magnetic wavelength up to $\sim 200\ \mu\mathrm{m}$, and we begin to see the development of longitudinal modes and filament breaking at the center of the interaction. This evolution is consistent with the experimental proton radiographs obtained. In particular, it is worth noting that the highly non-linear phase and onset of filament breaking resemble the highly distorted filaments phase observed at 5.5 ns for 5 mm separation (Figure 3). The details of how the ordered Weibel-mediated filaments break and give rise to shock formation are still not well understood. These results indicate that further investigation of the experimental interaction at later times with longer (and more energetic) flows can provide critical information in this regard.

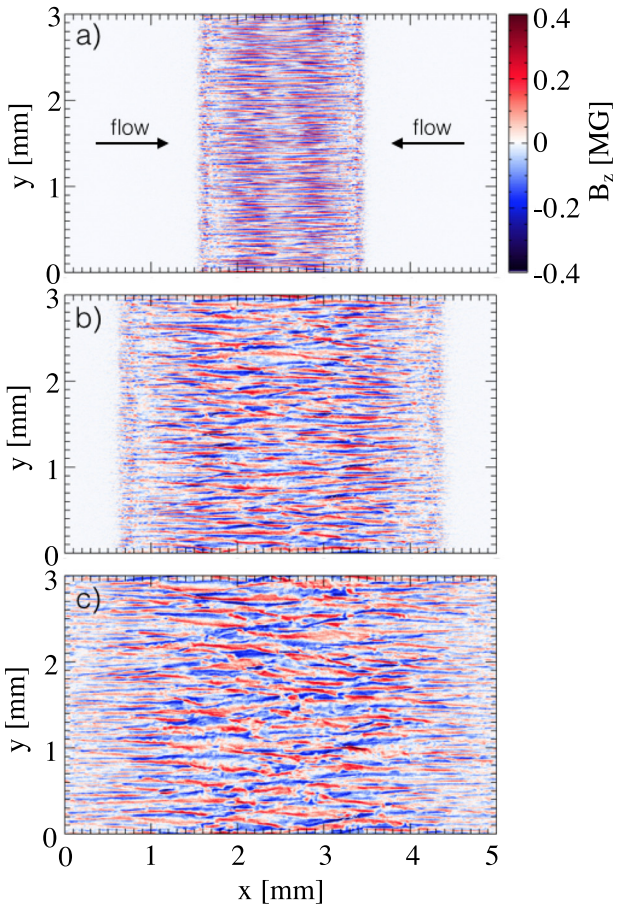

FIG. 5. 2D OSIRIS PIC simulation of the evolution of counter-streaming flows scaled to parameters relevant for the Omega experimental conditions ($v = 1000\,\mathrm{km/s}$, $n_e = 10^{19}\,\mathrm{cm}^{-3}$). The (out of page) magnetic field structure at (a) 3.3 ns, (b) 4.3 ns, and (c) 5.3 ns is shown. The arrows in (a) indicate the direction of the plasma flows.

IV. CONCLUSION

Beginning with a well-tested platform for generating collisionless plasma flows on the OMEGA Laser, we have changed the geometry in order to increase the plasma density in the flows. Using Thomson scattering, we measured an increase in ion density by a factor of approximately 4 over those previous experiments. This increased density leads to a fast development of Weibel instability, which was recorded using proton imaging. In addition to observing the clear development of strong and filamentary magnetic field structures, we have studied the rate at which the wavelength of the magnetic field filaments changes in the non-linear phase of the instability. While the rate of filament merging (as measured by the increase in wavelength) at higher density was comparable to the case of lower density for early times, we measure a continuous increase in the filament wavelength over several ns of observation in the higher density case. The fraction of the interaction volume subject to filamentation was also seen to continue to grow. By eschewing the fast, low-density flows of a truly collisionless system, this configuration is only marginally collisionless, but provides optimized conditions for the investigation of the non-linear development of the Weibel instability.

Going forward, generating a fully formed collisionless shock in the laboratory will require that the flows be highly collisionless ($L_{int}/\lambda_{mfp} \ll 1$) and that the Weibel instability reaches the non-linear regime within the bounds of the experiment ($L_{int}/(c/\omega_{pi}) \gg 200$).[27] These conditions can be simultaneously fulfilled by increasing the flow velocity and density in the interacting region, which strongly increases the mean free path ($\lambda_{mfp} \propto v^4/n$) while decreasing the ion skin depth ($c/\omega_{pi} \propto n^{-1/2}$). This combination is possible on the National Ignition Facility (NIF), due to the greater energy, length, and timescales available as compared to OMEGA. NIF experiments have already demonstrated increased density ($n_e > 10^{20}\,\mathrm{cm}^{-3}$) and $\sim 1000\,\mathrm{km/s}$ flows for foil separations in the range 6–10 mm.[47] Future work will further increase both density and velocity scales to create and study fully formed collisionless shocks in the laboratory for the first time.

ACKNOWLEDGMENTS

This work was performed under the auspices of the U.S. Department of Energy by Lawrence Livermore National Laboratory under Contract No. DE-AC52-07NA27344 and was partially funded by the Laboratory Directed Research and Development Program under project tracking code 15-ERD-065. This work was also supported by DOE FES under FWP 100237. F.F. acknowledges the OSIRIS Consortium, consisting of UCLA and IST (Portugal) for the use of the OSIRIS 3.0 framework and the visXD framework. OSIRIS simulations were run on Mira (ALCF) through an INCITE award.

[1]M. Ackermann, M. Ajello, A. Allafort, L. Baldini, J. Ballet, G. Barbiellini, M. G. Baring, D. Bastieri, K. Bechtol, R. Bellazzini, R. D. Blandford, E. D. Bloom, E. Bonamente, A. W. Borgland, E. Bottacini, T. J. Brandt, J. Bregeon, M. Brigida, P. Bruel, R. Buehler, G. Busetto, S. Buson, G. A. Caliandro, R. A. Cameron, P. A. Caraveo, J. M. Casandjian, C. Cecchi, Ö. Çelik, E. Charles, S. Chaty, R. C. G. Chaves, A. Chekhtman, C. C. Cheung, J. Chiang, G. Chiaro, A. N. Cillis, S. Ciprini, R. Claus, J. Cohen-Tanugi, L. R. Cominsky, J. Conrad, S. Corbel, S. Cutini, F. D'Ammando, A. de Angelis, F. de Palma, C. D. Dermer, E. do Couto e Silva, P. S. Drell, A. Drlica-Wagner, L. Falletti, C. Favuzzi, E. C. Ferrara, A. Franckowiak, Y. Fukazawa, S. Funk, P. Fusco, F. Gargano, S. Germani, N. Giglietto, P. Giommi, F. Giordano, M. Giroletti, T. Glanzman, G. Godfrey, I. A. Grenier, M.-H. Grondin, J. E. Grove, S. Guiriec, D. Hadasch, Y. Hanabata, A. K. Harding, M. Hayashida, K. Hayashi, E. Hays, J. W. Hewitt, A. B. Hill, R. E. Hughes, M. S. Jackson, T. Jogler, G. Jóhannesson, A. S. Johnson, T. Kamae, J. Kataoka, J. Katsuta, J. Knödlseder, M. Kuss, J. Lande, S. Larsson, L. Latronico, M. Lemoine-Goumard, F. Longo, F. Loparco, M. N. Lovellette, P. Lubrano, G. M. Madejski, F. Massaro, M. Mayer, M. N. Mazziotta, J. E. McEnery, J. Mehault, P. F. Michelson, R. P. Mignani, W. Mitthumsiri, T. Mizuno, A. A. Moiseev, M. E. Monzani, A. Morselli, I. V. Moskalenko, S. Murgia, T. Nakamori, R. Nemmen, E. Nuss, M. Ohno, T. Ohsugi, N. Omodei, M. Orienti, E. Orlando, J. F. Ormes, D. Paneque, J. S. Perkins, M. Pesce-Rollins, F. Piron, G. Pivato, S. Rainò, R. Rando, M. Razzano, S. Razzaque, A. Reimer, O. Reimer, S. Ritz, C. Romoli, M. Sánchez-Conde, A. Schulz, C. Sgrò, P. E. Simeon, E. J. Siskind, D. A. Smith, G. Spandre, P. Spinelli, F. W. Stecker, A. W. Strong, D. J. Suson, H. Tajima, H. Takahashi, T. Takahashi, T. Tanaka, J. G. Thayer, J. B. Thayer, D. J. Thompson, S. E. Thorsett, L. Tibaldo, O. Tibolla, M. Tinivella, E. Troja, Y. Uchiyama, T. L. Usher, J. Vandenbroucke, V. Vasileiou, G. Vianello, V. Vitale, A. P. Waite, M. Werner, B. L. Winer, K. S. Wood, M. Wood, R. Yamazaki, Z. Yang, and S. Zimmer, "Detection of the characteristic pion-decay signature in supernova remnants," Science **339**(6121), 807–811 (2013).

[2]R. Blandford and D. Eichler, "Particle acceleration at astrophysical shocks: A theory of cosmic ray origin," Phys. Rep. **154**, 1–75 (1987).

[3]A. Spitkovsky, "Particle acceleration in relativistic collisionless shocks: Fermi process at last?," Astrophys. J. Lett. **682**(1), L5–L8 (2008).

[4]J. S. Warren, J. P. Hughes, C. Badenes, P. Ghavamian, C. F. McKee, D. Moffett, P. P. Plucinsky, C. Rakowski, E. Reynoso, and P. Slane, "Cosmic-ray acceleration at the forward shock in Tycho's supernova remnant: Evidence from Chandra x-ray observations," Astrophys. J. **634**(1), 376 (2005).

[5]C. B. Hededal, T. Haugbølle, J. Trier Frederiksen, and Å. Nordlund, "Non-fermi power-law acceleration in astrophysical plasma shocks," Astrophys. J. Lett. **617**(2), L107 (2004).

[6]S. F. Martins, R. A. Fonseca, L. O. Silva, and W. B. Mori, "Ion dynamics and acceleration in relativistic shocks," Astrophys. J. Lett. **695**(2), L189–L193 (2009).

[7]M. V. Medvedev and O. V. Zakutnyaya, "Magnetic fields and cosmic rays in GRBs: A self-similar collisionless foreshock," Astrophys. J. **696**(2), 2269 (2009).

[8]K. A. Eriksen, J. P. Hughes, C. Badenes, R. Fesen, P. Ghavamian, D. Moffett, P. P. Plucinksy, C. E. Rakowski, E. M. Reynoso, and P. Slane, "Evidence for particle acceleration to the knee of the cosmic ray spectrum in Tycho's supernova remnant," Astrophys. J. Lett. **728**(2), L28 (2011).

[9]E. S. Weibel, "Spontaneously growing transverse waves in a plasma due to an anisotropic velocity distribution," Phys. Rev. Lett. **2**, 83–84 (1959).

[10]C. Courtois, R. A. D. Grundy, A. D. Ash, D. M. Chambers, N. C. Woolsey, R. O. Dendy, and K. G. McClements, "Experiment on collisionless plasma interaction with applications to supernova remnant physics," Phys. Plasmas **11**(7), 3386–3393 (2004).

[11]L. Gargate, R. A. Fonseca, J. Niemiec, M. Pohl, R. Bingham, and L. O. Silva, "The nonlinear saturation of the non-resonant kinetically driven streaming instability," Astrophys. J. Lett. **711**(2), L127 (2010).

[12]J. Niemiec, M. Pohl, T. Stroman, and K.-I. Nishikawa, "Production of magnetic turbulence by cosmic rays drifting upstream of supernova remnant shocks," Astrophys. J. **684**(2), 1174 (2008).

[13]A. Bret, "Weibel, two-stream, filamentation, oblique, bell, buneman… which one grows faster?," Astrophys. J. **699**(2), 990 (2009).

[14]C. Constantin, W. Gekelman, P. Pribyl, E. Everson, D. Schaeffer, N. Kugland, R. Presura, S. Neff, C. Plechaty, S. Vincena, A. Collette, S. Tripathi, M. Villagran Muniz, and C. Niemann, "Collisionless interaction of an energetic laser produced plasma with a large magnetoplasma," Astrophys. Space Sci. **322**(1), 155–159 (2009).

[15]G. Fiksel, W. Fox, A. Bhattacharjee, D. H. Barnak, P.-Y. Chang, K. Germaschewski, S. X. Hu, and P. M. Nilson, "Magnetic reconnection between colliding magnetized laser-produced plasma plumes," Phys. Rev. Lett. **113**, 105003 (2014).

[16]S. E. Clark, E. T. Everson, D. B. Schaeffer, A. S. Bondarenko, C. G. Constantin, C. Niemann, and D. Winske, "Enhanced collisionless shock formation in a magnetized plasma containing a density gradient," Phys. Rev. E **90**, 041101 (2014).

[17]J. Pruet, K. Abazajian, and G. M. Fuller, "New connection between central engine weak physics and the dynamics of gamma-ray burst fireballs," Phys. Rev. D **64**, 063002 (2001).

[18]M. Fiore, L. O. Silva, C. Ren, M. A. Tzoufras, and W. B. Mori, "Baryon loading and the Weibel instability in gamma-ray bursts," Mon. Not. R. Astron. Soc. **372**(4), 1851 (2006).

[19]M. V. Medvedev, L. O. Silva, M. Fiore, R. A. Fonseca, and W. B. Mori, "Generation of magnetic fields in cosmological shocks," J. Korean Astron. Soc. **37**(5), 533–541 (2004).

[20]M. V. Medvedev and A. Loeb, "Generation of magnetic fields in the relativistic shock of gamma-ray burst sources," Astrophys. J. **526**(2), 697–706 (1999).

[21]A. Gruzinov and E. Waxman, "Gamma-ray burst afterglow: Polarization and analytic light curves," Astrophys. J. **511**, 852–861 (1999).

[22]M. V. Medvedev and A. Spitkovsky, "Radiative cooling in relativistic collisionless shocks: Can simulations and experiments probe relevant gamma-ray burst physics?," Astrophys. J. **700**(2), 956 (2009).

[23]M. V. Medvedev, D. Lazzati, B. C. Morsony, and J. C. Workman, "Jitter radiation as a possible mechanism for gamma-ray burst afterglows: Spectra and light curves," Astrophys. J. **666**(1), 339 (2007).

[24]M. V. Medvedev, "The theory of spectral evolution of the gamma-ray burst prompt emission," Astrophys. J. **637**(2), 869 (2006).

[25]L. O. Silva, R. A. Fonseca, J. W. Tonge, J. M. Dawson, W. B. Mori, and M. V. Medvedev, "Interpenetrating plasma shells: Near-equipartition magnetic field generation and nonthermal particle acceleration," Astrophys. J. Lett. **596**(1), L121 (2003).

[26]J. Trier Frederiksen, C. B. Hededal, T. Haugbølle, and Å. Nordlund, "Magnetic field generation in collisionless shocks: Pattern growth and transport," Astrophys. J. Lett. **608**(1), L13 (2004).

[27]T. N. Kato and H. Takabe, "Nonrelativistic collisionless shocks in unmagnetized electron-ion plasmas," Astrophys. J. Lett. **681**(2), L93–L96 (2008).

[28]K.-I. Nishikawa, P. Hardee, G. Richardson, R. Preece, H. Sol, and G. J. Fishman, "Particle acceleration in relativistic jets due to Weibel instability," Astrophys. J. **595**(1), 555 (2003).

[29]S. Kneip, C. McGuffey, J. L. Martins, S. F. Martins, C. Bellei, V. Chvykov, F. Dollar, R. Fonseca, C. Huntington, G. Kalintchenko, A. Maksimchuk, S. P. D. Mangles, T. Matsuoka, S. R. Nagel, C. A. J. Palmer, J. Schreiber, K. Ta Phuoc, A. G. R. Thomas, V. Yanovsky, L. O. Silva, K. Krushelnick, and Z. Najmudin, "Bright spatially coherent synchrotron x-rays from a table-top source," Nat. Phys. **6**(12), 980–983 (2010).

[30]C. M. Huntington, A. G. R. Thomas, C. McGuffey, T. Matsuoka, V. Chvykov, G. Kalintchenko, S. Kneip, Z. Najmudin, C. Palmer, V. Yanovsky, A. Maksimchuk, R. P. Drake, T. Katsouleas, and K. Krushelnick, "Current filamentation instability in laser wakefield accelerators," Phys. Rev. Lett. **106**(10), 105001 (2011).

[31]B. Allen, V. Yakimenko, M. Babzien, M. Fedurin, K. Kusche, and P. Muggli, "Experimental study of current filamentation instability," Phys. Rev. Lett. **109**, 185007 (2012).

[32]J. S. Ross, S. H. Glenzer, P. Amendt, R. Berger, L. Divol, N. L. Kugland, O. L. Landen, C. Plechaty, B. Remington, D. Ryutov, W. Rozmus, D. H. Froula, G. Fiksel, C. Sorce, Y. Kuramitsu, T. Morita, Y. Sakawa, H. Takabe, R. P. Drake, M. Grosskopf, C. Kuranz, G. Gregori, J. Meinecke, C. D. Murphy, M. Koenig, A. Pelka, A. Ravasio, T. Vinci, E. Liang, R. Presura, A. Spitkovsky, F. Miniati, and H.-S. Park, "Characterizing counter-streaming interpenetrating plasmas relevant to astrophysical collisionless shocks," Phys. Plasmas **19**(5), 056501 (2012).

[33]H.-S. Park, C. M. Huntington, F. Fiuza, R. P. Drake, D. H. Froula, G. Gregori, M. Koenig, N. L. Kugland, C. C. Kuranz, D. Q. Lamb, M. C. Levy, C. K. Li, J. Meinecke, T. Morita, R. D. Petrasso, B. B. Pollock, B. A. Remington, H. G. Rinderknecht, M. Rosenberg, J. S. Ross, D. D. Ryutov, Y. Sakawa, A. Spitkovsky, H. Takabe, D. P. Turnbull, P. Tzeferacos, S. V. Weber, and A. B. Zylstra, "Collisionless shock experiments with lasers and observation of Weibel instabilities," Phys. Plasmas **22**(5), 056311 (2015).

[34]C. M. Huntington, F. Fiuza, J. S. Ross, A. B. Zylstra, R. P. Drake, D. H. Froula, G. Gregori, N. L. Kugland, C. C. Kuranz, M. C. Levy, C. K. Li, J.

Meinecke, T. Morita, R. Petrasso, C. Plechaty, B. A. Remington, D. D. Ryutov, Y. Sakawa, A. Spitkovsky, H. Takabe, and H. S. Park, "Observation of magnetic field generation via the Weibel instability in interpenetrating plasma flows," Nat. Phys. **11**(2), 173–176 (2015).

[35]J. S. Ross, H.-S. Park, R. Berger, L. Divol, N. L. Kugland, W. Rozmus, D. Ryutov, and S. H. Glenzer, "Collisionless coupling of ion and electron temperatures in counterstreaming plasma flows," Phys. Rev. Lett. **110**, 145005 (2013).

[36]M. J.-E. Manuel, A. B. Zylstra, H. G. Rinderknecht, D. T. Casey, M. J. Rosenberg, N. Sinenian, C. K. Li, J. A. Frenje, F. H. Séguin, and R. D. Petrasso, "Source characterization and modeling development for monoenergetic-proton radiography experiments on omega," Rev. Sci. Instrum. **83**(6), 063506 (2012).

[37]N. L. Kugland, D. D. Ryutov, P.-Y. Chang, R. P. Drake, G. Fiksel, D. H. Froula, S. H. Glenzer, G. Gregori, M. Grosskopf, M. Koenig, Y. Kuramitsu, C. Kuranz, M. C. Levy, E. Liang, J. Meinecke, F. Miniati, T. Morita, A. Pelka, C. Plechaty, R. Presura, A. Ravasio, B. A. Remington, B. Reville, J. S. Ross, Y. Sakawa, A. Spitkovsky, H. Takabe, and H-S. Park, "Self-organized electromagnetic field structures in laser-produced counter-streaming plasmas," Nat. Phys. **8**(11), 809–812 (2012).

[38]N. L. Kugland, J. S. Ross, P.-Y. Chang, R. P. Drake, G. Fiksel, D. H. Froula, S. H. Glenzer, G. Gregori, M. Grosskopf, C. Huntington, M. Koenig, Y. Kuramitsu, C. Kuranz, M. C. Levy, E. Liang, D. Martinez, J. Meinecke, F. Miniati, T. Morita, A. Pelka, C. Plechaty, R. Presura, A. Ravasio, B. A. Remington, B. Reville, D. D. Ryutov, Y. Sakawa, A. Spitkovsky, H. Takabe, and H.-S. Park, "Visualizing electromagnetic fields in laser-produced counter-streaming plasma experiments for collisionless shock laboratory astrophysics," Phys. Plasmas **20**(5), 056313 (2013).

[39]D. D. Ryutov, F. Fiuza, C. M. Huntington, J. S. Ross, and H.-S. Park, "Collisional effects in the ion Weibel instability for two counter-propagating plasma streams," Phys. Plasmas **21**(3), 032701 (2014).

[40]C. K. Li, F. H. Séguin, J. A. Frenje, J. R. Rygg, R. D. Petrasso, R. P. J. Town, P. A. Amendt, S. P. Hatchett, O. L. Landen, A. J. Mackinnon, P. K. Patel, V. A. Smalyuk, J. P. Knauer, T. C. Sangster, and C. Stoeckl, "Monoenergetic proton backlighter for measuring e and b fields and for radiographing implosions and high-energy density plasmas (invited)," Rev. Sci. Instrum. **77**(10), 10E725 (2006).

[41]M. C. Levy, D. D. Ryutov, S. C. Wilks, J. S. Ross, C. M. Huntington, F. Fiuza, D. A. Martinez, N. L. Kugland, M. G. Baring, and H.-S. Park, "Development of an interpretive simulation tool for the proton radiography technique," Rev. Sci. Instrum. **86**(3), 033302 (2015).

[42]N. L. Kugland, D. D. Ryutov, C. Plechaty, J. S. Ross, and H.-S. Park, "Invited article: Relation between electric and magnetic field structures and their proton-beam images," Rev. Sci. Instrum. **83**(10), 101301 (2012).

[43]M. M. Marinak, R. E. Tipton, O. L. Landen, T. J. Murphy, P. Amendt, S. W. Haan, S. P. Hatchett, C. J. Keane, R. McEachern, and R. Wallace, "Three-dimensional simulations of nova high growth factor capsule implosion experiments," Phys. Plasmas **3**(5), 2070–2076 (1996).

[44]R. Fonseca, L. Silva, F. Tsung, V. Decyk, W. Lu, C. Ren, W. Mori, S. Deng, S. Lee, T. Katsouleas, and J. Adam, "Osiris: A three-dimensional, fully relativistic particle in cell code for modeling plasma based accelerators," in *Computational Science, ICCS 2002*, Lecture Notes in Computer Science Vol. 2331, edited by P. Sloot, A. Hoekstra, C. Tan, and J. Dongarra (Springer, Berlin, Heidelberg, 2002), pp. 342–351.

[45]R. A. Fonseca, S. F. Martins, L. O. Silva, J. W. Tonge, F. S. Tsung, and W. B. Mori, "One-to-one direct modeling of experiments and astrophysical scenarios: Pushing the envelope on kinetic plasma simulations," Plasma Phys. Controlled Fusion **50**(12), 124034 (2008).

[46]D. D. Ryutov, N. L. Kugland, H. S. Park, C. Plechaty, B. A. Remington, and J. S. Ross, "Basic scalings for collisionless-shock experiments in a plasma without pre-imposed magnetic field," Plasma Phys. Controlled Fusion **54**(10), 105021 (2012).

[47]J. S. Ross, D. P. Higginson, D. Ryutov, F. Fiuza, R. Hatarik, C. M. Huntington, D. H. Kalantar, A. Link, B. B. Pollock, B. A. Remington, H. G. Rinderknecht, G. F. Swadling, D. P. Turnbull, S. Weber, S. Wilks, D. H. Froula, M. J. Rosenberg, T. Morita, Y. Sakawa, H. Takabe, R. P. Drake, C. Kuranz, G. Gregori, J. Meinecke, M. C. Levy, M. Koenig, A. Spitkovsky, R. D. Petrasso, C. K. Li, H. Sio, B. Lahmann, A. B. Zylstra, and H.-S. Park, "Transition from collisional to collisionless regimes in interpenetrating plasma flows on the national ignition facility," Phys. Rev. Lett. (to be published).